Chinese Journal of Chemical Engineering 54 (2023) 29–35

Contents lists available at ScienceDirect

Chinese Journal of Chemical Engineering

journal homepage: www.elsevier.com/locate/CJChE

Full Length Article

Multi-scale simulation of diffusion behavior of deterrent in propellant

Pan Huang [1,#], Zekai Zhang [2,#], Yuxin Chen [1], Changwei Liu [1], Yong Zhang [3], Cheng Lian [1,2,*], Yajun Ding [3,*], Honglai Liu [1,2]

[1] State Key Laboratory of Chemical Engineering, Shanghai Engineering Research Center of Hierarchical Nanomaterials, School of Chemical Engineering, East China University of Science and Technology, Shanghai 200237, China
[2] School of Chemistry and Molecular Engineering, East China University of Science and Technology, Shanghai 200237, China
[3] School of Chemistry and Chemical Engineering, Nanjing University of Science and Technology, Nanjing 210094, China

ARTICLE INFO

Article history:
Received 13 September 2021
Received in revised form 17 March 2022
Accepted 28 March 2022
Available online 1 April 2022

Keywords:
Multi-scale simulation
Diffusion
Deterrent
Propellant
Onion model
Molecular dynamics simulation

ABSTRACT

Concentration distribution of the deterrent in single-base propellant during the process of firing plays an important role in the ballistic properties of gun propellant in weapons. However, the diffusion coefficient calculated by molecular dynamics (MD) simulation is 6 orders of magnitude larger than the experimental values. Meanwhile, few simple and comprehensive theoretical models can explain the phenomenon and accurately predict the concentration distribution of the propellant. Herein, an onion model combining with MD simulation and finite element method of diffusion in propellants is introduced to bridge the gap between the experiments and simulations, and correctly predict the concentration distribution of deterrent. Furthermore, a new time scale is found to characterize the diffusion process. Finally, the time- and position-depended concentration distributions of dibutyl phthalate in nitrocellulose are measured by Raman spectroscopy to verify the correctness of the onion model. This work not only provides guidance for the design of the deterrent, but could be also extended to the diffusion of small molecules in polymer with different crystallinity.

1. Introduction

As an important part of barrel weapon, propellant contains oxidizing and combustible components, which provide power for projectile ejection. The single-base propellant is widely used with excellent performance, suitable for medium and small caliber guns and mortar charges [1,2]. A gradient distribution of deterrent in the propellant is proposed to reduce the burning rate of propellant for improving the ballistic performance, such as lower bore pressure and higher initial velocity [3]. In addition, the diffusion of the deterrent during the long storage will also directly affect the service life of the single-base propellant [4]. Therefore, the measurement and control of concentration distribution and diffusion of deterrent in the single-base propellant is the key to improving the ballistic performance of propellant [5].

Measuring the concentration distribution of deterrent by experimental methods have undergone several decades of development. In the 1970s, an auto radio graphic determination was developed to determine the distribution of deterrent concentration insensitive gunpowder with isotope labeling [6]. In the 1980s, an analytical method based on centrifugal sand milling was established to separate drug granules layer by layer. In recent years, solvent extraction [7], gas chromatography [8], and FTIR microspectroscopy [9] have been developed. However, for the sake of sampling difficulty caused by the thickness of only ten to several hundred microns, most of these methods cannot obtain reliable and stable concentration distribution of deterrent. What's more, the sectioning procedure can destroy propellant, resulting in inaccurate measurement results. These disadvantages make it difficult to study the concentration distribution of gunpowder by experimental method.

Fortunately, computer simulation [10,11] largely overcomes the defect and decreases the experiment time and reduces the experiment cost. Takeuchi *et al.* [12] simulated the diffusion of simple gas molecules in a chain polymer. The simulation depends on the relationship between diffusion and free volume. Zhang *et al.* [13] simulated the adsorption behavior and mechanism of neutral polymer binder in nitrate ester plasticized polyether propellant by molecular dynamics. The results show that neutral polymer

* Corresponding authors.
E-mail addresses: liancheng@ecust.edu.cn (C. Lian), dyj@njust.edu.cn (Y. Ding).
# These authors contributed equally to this article.

https://doi.org/10.1016/j.cjche.2022.03.018
1004-9541/

binder can enhance the interfacial strength of propellant. Although MD simulation can accurately calculate many properties of polymers, the diffusion coefficient D of guest molecules in polymers obtained by MD simulation differs greatly from that from the experiment. Wei *et al.* [8] simulated the diffusion behavior of small molecule deterrent in the single-base propellant, finding the diffusion coefficient obtained by MD simulation is about 6 times larger than that measured by experiment. Ding *et al.* [14]simulated the diffusion of dibutyl phthalate (DBP) in polyneopentyl glycol adipate with the changes of temperature. The diffusion coefficient was about 5 times larger than that measured in the experiment. Therefore, MD simulation alone cannot accurately describe the diffusion behavior of deterrent in propellant by MD simulation.

To solve this problem, many theoretical models are established. Gennes *et al.* [15]put forward the pupal movement model. However, the model is rough to obtain the concentration distribution at a certain time. Brodman *et al.* proposed a model considering the intra molecular hydrogen bonds. The concentration distribution curve of the deterrent is stepped and completely different from the classical Fick's law [16]. Nevertheless, this model cannot explain the effect of propellant crystallization on diffusion. Therefore, it is crucial to propose a model considering the effects of crystallization and internal interaction affecting the diffusion of the deterrent.

In this work, we developed an onion model, considering degrees of crystallinity and intermolecular hydrogen bonding forces in propellants. The flow diagram is shown in Fig. 1. Firstly, the diffusion coefficients D of DBP in nitrocellulose (NC) at different temperatures are calculated by MD simulation. Meanwhile, the diffusion activation energy and intrinsic diffusion coefficient D_F are calculated by the Arrhenius equation. In addition, combining D with the onion model, we obtain the equivalent diffusion path length of DBP in the propellant, the relaxation time of diffusion, and the concentration distribution of deterrent at any time and any position. Finally, we measure the concentration distribution of deterrent in propellant after a certain aging process by Raman spectroscopy. The accuracy of the onion model was verified by comparing it with the experimental data. This work can provide ideas for the simulation of the diffusion of small molecules in the polymer of different crystallinity, and can better guide the development of deterrent in propellant theoretically.

2. Method and Models

2.1. MD simulation for the diffusion coefficient

MD simulation relies on classical mechanics to calculate the equilibrium process and transfer properties of a large number of molecules. MD based on classical mechanics is more accurate and physically meaningful than Monte Carlo method based on statistics in calculating diffusion coefficients. Moreover, with the development of modern computer technology, the speed of MD simulation is getting faster and faster. The micro system calculated by MD simulation is defined by the density and composition of the propellant, which is obtained from experiment. The details of model construction are as follows:

At first, the Forcite module [17] is used to optimize the structure of molecules and determine the charge of each atom. Relevant parameters are set as follows: Geometry optimization for task selection, ultra-fine precision for convergence, the smart method by default for algorithm; COMPASSII [18] for the force field, it is suitable for most of the organic matter, inorganic matter, metal oxides and halide, charge choose force field assigned, ultra-fine for energy calculation accuracy; Ewald & Grou [19] for electrostatic, atom-based for van der Waals. The optimized molecular structures are shown in Fig. 1(a).

Then amorphous cell module [20] is used to build the structure of a certain concentration of DBP and NC. Relevant parameters are set as follows: Construction for task selection, ultra-fine precision for convergence; 2 NC chains with a polymerization degree of 10 and 36 DBP molecules are built, with a total number of 1782 of atoms. 298 K for temperature, 1 for the geometric configuration number, 1.07 g·cm^{-3} for initial density. Moreover, the Forcite module is used to minimize the energy of the whole system.

Finally, use the dynamics function of the Forcite module to perform the dynamic module. The parameters of MD simulation are as follows: NVT ensemble was used, Nose for the thermostat, COMPASSII for the force field, the initial velocity was random and sampled from Maxwell–Boltzmann distribution. The temperature was selected as 293–353 K, the simulated step size was 1 fs, the simulated step number was 50000, the overall simulation time was 50 ps, and the image was output every 5000 steps for the analysis of diffusion results; MD simulation was performed again with the results of the previous step, NVT ensemble was used, the initial velocity was current, the simulated step number was 1000000, and the overall simulation time was 1000 ps.

Consider the mean value of particle displacement squared as mean squared displacement (MSD, m^2):

$$\mathrm{MSD} = R(t) = \left\langle |\boldsymbol{r}(t) - \boldsymbol{r}(0)|^2 \right\rangle \tag{1}$$

where $\boldsymbol{r}(0)$ and $\boldsymbol{r}(t)$ (m) represent the positions of the center of mass of molecules at time 0 and t (ps), respectively. The diffusion coefficient D can be obtained according to the Einstein–Smoluchowski equation:

$$D = \lim_{t\to\infty} \frac{\left\langle |\boldsymbol{r}(t) - \boldsymbol{r}(0)|^2 \right\rangle}{6t} \tag{2}$$

Material Studio 8.0 is used to build the structure of a certain concentration of DBP and NC and MD simulation.

2.2. Onion model

The internal crystal structure of propellant is very complex, and diffusion of small molecules in propellant only occurs in the amorphous region, but not the crystal region [21–23] (the internal crystallization diagram of propellant is shown in Supplementary Material S1 (S1)). Therefore, an onion model is constructed to simulate the diffusion of DBP in NC by considering the crystallization of NC, as shown in Fig. 1(b).

The macro system (onion model) is based on the cross-section of the cylindrical propellant and its radius is R (the simulation value is 1 mm). The clapboards inside the onion model simulate the crystallization in the propellant. DBP cannot diffuse through the clapboards, and the number of clapboard layers is n. The number of holes for the diffusion of small molecules in each layer of clapboards is m. The perforating rate of each clapboard is ε and the arrangement of holes is uniform. Fig. 1(b) is a schematic diagram of the onion model of $n = 5$ and $m = 4$.

Without considering the factor of crystallization, DBP will diffuse radially to the center of the propellant. In the onion model, the DBP will bypass the clapboards and increase the diffusion distance, which is marked as the equivalent diffusion distance R_{eff}. The equivalent diffusion path is shown in Fig. 1(b). Furthermore, the diffusion distance of DBP in each layer of the onion model is an arithmetic sequence, R_{eff} can be derived by m and n as (specific derivation process is detailed in S2):

$$R_{\mathrm{eff}} = \frac{\pi R(n-1)}{2m} + R \tag{3}$$

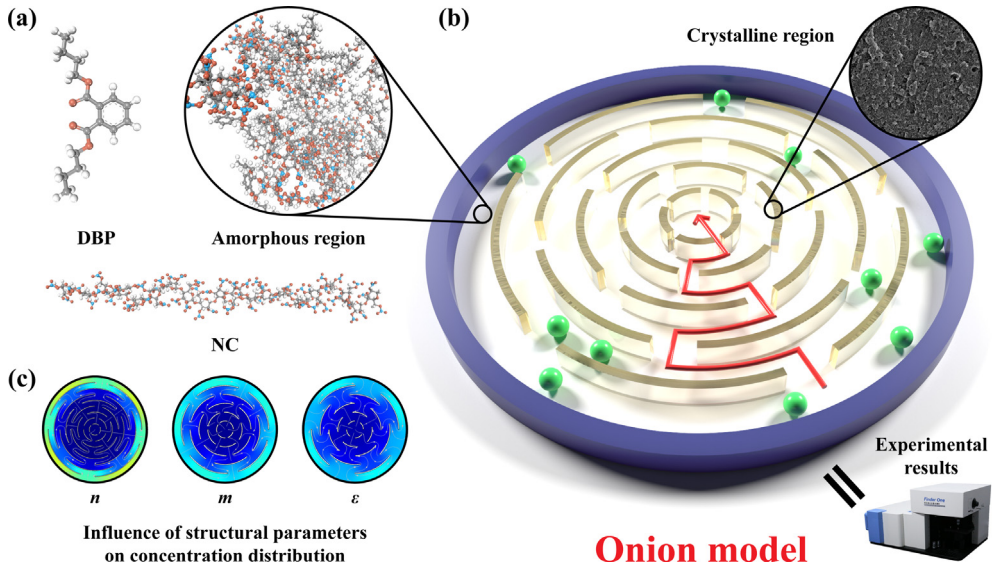

Fig. 1. The flow diagram of onion model design and comparison with experiment. (a) The amorphous region of propellant, which is consisted of DBP and NC. (b) The schematic diagram of the onion model. The crystal region is represented by clapboards. The red line represents the motion path of small molecule deterrent molecules in the amorphous region, n represents the number of layers of clapboards, m represents the numbers of holes in each layer of clapboards, and ε represents the perforating rate of each layer of clapboards. (c) Concentration distribution under different structural parameters of the onion model at 1 h.

At the same time, the relaxation time of diffusion can be dimensionless by m, n in the onion model and temperature T in the diffusion process as follow:

$$\tau = \frac{R^2}{D} = \frac{R_{\text{eff}}^2}{D_{\text{eff}}} \tag{4}$$

Therefore, we can get D_{eff} from a series of experimental data, which will combine with the data from MD simulation to get the variable R_{eff} by Eq. (4). Then, through importing R_{eff} into Eq. (3), we can get m and n, where m and n represent the internal crystallization of propellant and various interaction forces. So that the diffusion coefficient of the onion model can be consistent with the actual diffusion coefficient.

2.3. The Fick's law for the concentration distribution

The Fick's law describes the relationship between the diffusion flux and concentration gradient in the process of molecular diffusion when diffusion phenomenon occurs without macroscopic mixing. The diffusion flux $\boldsymbol{J}$ through the unit area perpendicular to the diffusion direction per unit time is proportional to the concentration gradient ∇c $(\text{mol}\cdot\text{m}^{-4})$ at the cross-section. The formula is expressed as:

$$\boldsymbol{J} = -D\nabla c \tag{5}$$

In the unsteady diffusion process, the rate of change of the concentration with time $\partial c/\partial t$ is equal to the inverse of the gradient of diffusion flux. The Fick's second law is expressed as:

$$\frac{\delta C_{\text{p}}}{\delta t} = D_{\text{eff}} \frac{\partial^2 C_{\text{p}}}{\partial x^2} \tag{6}$$

where C_{p} is the concentration of plasticizer in the polymer at time t and D_{eff} is a constant.

By using Fick's law diffusion model and the corresponding initial and boundary conditions, the concentration distribution of the deterrent at any position of propellant and at any time can be obtained. The boundary condition of the desensitization process is that the concentration of the external deterrent is kept constant. The boundary condition of the aging process is that the concentration of the external deterrent is 0 and the deterrent inside the propellant diffuses outward at a diffusion velocity. The initial condition of the desensitization process is that the concentration of the deterrent in the propellant is 0, and the initial condition of the aging process is the concentration of the propellant through the desensitization process.

Because of the existence of clapboard in the onion model, the DPB concentration distribution at the same distance from the center is different. Similarly, in the simulation process of deterrent in the propellant, the ordering of its X and Y coordinates is irregular, so it is not realistic to count and integrate them manually. To solve this problem, a Python script (the specific script is displayed in S3) is written to count and integrate the calculation results. The outer contour of the geometric model used in the numerical calculation is a circle with a radius of 1 mm, which is divided into N segments. When integrating the calculation results, the i segment represents a ring with a radial length of $R_{i-1} - R_i$ and the relationship between R_i and i is as follows:

$$R_i = \frac{i}{N} \tag{7}$$

the corresponding radial position depth is as follows:

$$\text{Depth} = 1 - \frac{R_{i-1} + R_i}{2} \tag{8}$$

Through the Python script, after all the DBP concentrations of all the lattice points are screened into the statistical list, the geometric average of all the values in each statistical list is obtained, that is, the DBP concentration in a certain radial range. Finally, N radial range values and corresponding DBP concentration values are output for subsequent curve drawing. So far, the radial distribution data of DBP concentration are obtained on the premise of ensuring the rationality of the calculation results.

The integrated development environment adopted is PyCharm, Python version 3.9.1, and math and matplotlib toolkits are loaded in the script.

COMSOL Multiphysics 5.3 is used to build the construction of the onion model and the finite element simulation. The integrated development environment adopted is PyCharm, Python version 3.9.1, and math and matplotlib toolkits are loaded in the script.

2.4. Diffusion coefficient of DBP in NC by experiment

2.4.1. Experimental principle of measuring concentration distribution by Raman spectroscopy

As a new nondestructive testing technology, laser Raman spectroscopy is widely used in qualitative and quantitative analysis of samples. The instrument method is used to establish a direct, accurate, and rapid quantitative determination method of substance content in the propellant, which is of great significance for the study of propellant. The method has the advantages of simple determination, convenient operation, no damage to the sample, and no need to add other chemical reagents [24,25]. The formula of Raman spectrum quantitative analysis is as:

$$I = K\Phi X\int_0^b e^{(\ln 10)(k'+k)z}h(z)dz \tag{9}$$

In the formula: I is the Raman signal intensity of the sample surface collected by the optical system; K is the Raman scattering cross-sectional area of the molecule; Φ is the laser incident power on the sample surface; k and k' are the absorption coefficients of incident light and scattered light respectively; z is the distance between incident light and scattered light; $h(z)$ is the transfer function of the optical system; b is the thickness of the sample cell.

It can be seen from Eq. (9) that under certain conditions, the intensity of the Raman signal is proportional to the concentration of the substance to be measured. That is:

$$I \propto C \tag{10}$$

In the quantitative analysis, the analytical curves of spectral intensity and concentration are established at first, and then the samples are detected. Finally, the diffusion coefficient can be calculated by the second diffusion model (the specific calculation method is shown in S4).

2.4.2. Instruments and reagents

Micro confocal Raman spectrometer (Invia type, Renishaw, UK). Single-baseball tablet, NC (Luzhou North Chemical Industry Co., Ltd., China); DBP (analytical pure, Yonghua Chemical Technology Co., Ltd., China); ethyl acetate (analytical pure, Shanghai Wokai Biotechnology Co., Ltd., China).

Preparation of the standard sample: the single-base propellant was dissolved by ethyl acetate and evenly mixed with DBP and NC to prepare a series of standard samples with different deterrent content, poured into a petri dish, and made into a thin film after the solvent was evaporated. The concentration of NG is 10%, the concentration of DBP is 6.5%. The reaction temperatures were 328, 338 and 348 K, respectively, and aged for 6 days.

Preparation of samples to be tested: the samples of insensitive propellant after accelerated aging were cut into thin films with a thickness of 15 μm by using a frozen slicer.

2.4.3. Experimental procedures

Deterrent concentration distribution test: Fix the sample to be tested on a glass slide, and use the Renishaw company inVia Raman spectrometer to test the deterrent concentration distribution of the sample cut into thin films. The objective lens magnification is 50, the laser wavelength is 532 nm, and the laser power is 10%, exposure time 3 s, exposure times 1, spectrum collection range 600–4000 cm^{-1}.

3. Results and Discussion

3.1. Diffusion coefficient obtained by MD simulation

Fig. 2 and Table 1 show that from 50 ps to 900 ps, MSD has a strong linear relationship with time, satisfying the Einstein–Smoluchowski equation (the correlation coefficient is greater than 0.98). According to Eq. (2), the diffusion coefficient D is calculated and shown in Table 1. What's more, as the temperature increases, the slope of the fitted line (diffusion coefficient) increases, which is satisfied with the Arrhenius equation [26]:

$$D_F = D_0\exp(-\frac{E}{RT}) \tag{11}$$

where D_F represents intrinsic diffusion coefficient ($m^2{\cdot}s^{-1}$), D_0 represents pre-exponential factor ($m^2{\cdot}s^{-1}$), E represents diffusion activation energy ($J{\cdot}mol^{-1}$), R represents gas constant (8.314 $J{\cdot}mol^{-1}{\cdot}K^{-1}$), and T represents temperature (K).

Diffusion activation energy is the energy required for molecules to change from normal state to active state prone to diffusion movement. Arrhenius equation can well describe the relationship between diffusion coefficient and temperature, and can calculate diffusion activation energy [27–29].

We can obtain the diffusion activation energy and pre-exponential factor by 50–900 ps data fitting. According to the simulation data of DBP diffusion coefficient at different temperatures, ln$D$ was used to plot $1/T$ and perform linear fitting (Fig. 2). The fitting result is:

$$\ln D = -1817.44\times(1/T) - 16.91 \tag{11}$$

The specific results of fitting are shown in Table 2. The result shows that there is a strong linear correlation between ln D and $1/T$, and the correlation coefficient is 0.866. So, the diffusion coefficient and the temperature greatly satisfy the Arrhenius equation.

3.2. Concentration distribution calculated by onion model

Because the effect of internal crystallization is not taken into account, the diffusion coefficient obtained by MD simulation is much larger than the experimental range from 10^{-17} to 10^{-14} $m^2{\cdot}s^{-1}$ [30]. Therefore, the onion model is introduced to represent the internal crystallization of the propellant and bridge the gap between simulation and experiment.

To intuitively explore the effects of the n and m of the onion model and temperature T on the diffusion behavior of DBP in NC, the concentration distribution diagram at mesoscale is drawn. As shown in the illustration, the red part contains a high concentration of DBP, and the dark blue part does not contain DBP. From the concentration distribution schematic diagram, we can see that DBP diffuses from outside to inside, and the concentration distribution at the same depth is relatively uniform. From Figs. 3–5, the diffusion rate of DBP slows down with the number of clapboards from 2 to 10, with the increase of the number of holes in each clapboard and temperature, the diffusion rate of DBP becomes faster.

It can be seen from Eqs. (3) and (4) that the changes of equivalent radius R_{eff} are ultimately attributed to the changes of n and m, and the change of D_F is ultimately attributed to the change of temperature during diffusion. τ can be used to normalize different factors influencing diffusion. Fig. 6 shows the relationship between the maximum concentration and the minimum concentration of propellant with time. The results of Fig. 6(a)–(c) show that under the same initial concentration distribution condition, with the decrease of the number of clapboards, the number of pores in each clapboard increases and the temperature increases, and the maximum (minimum) concentration of the system decreases (increases) more slowly. And the time to reach the equilibrium

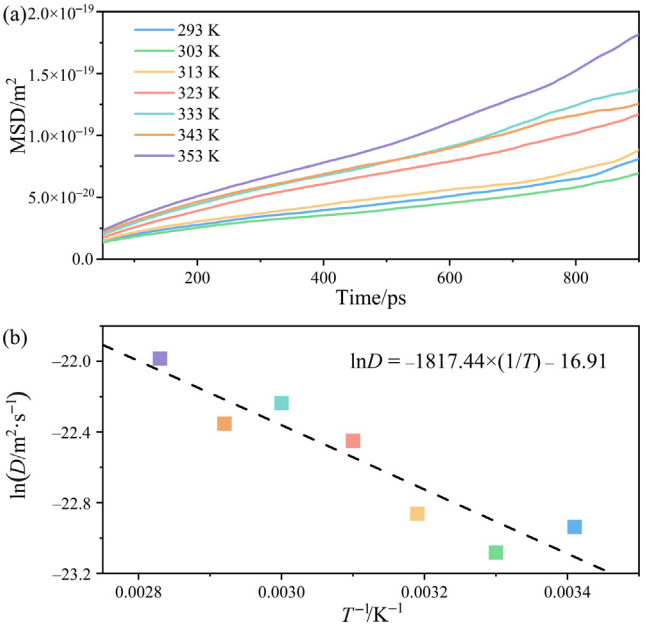

Fig. 2. (a) The curves of MSD with time. (b) The intrinsic diffusion coefficient is fitted to the function of temperature from 293 K to 353 K.

Table 1
MSD data analysis and the diffusion coefficients of DBP in 293–353 K

Temperature/ K	Slope × 10^{20}/ $m^2 \cdot s^{-1}$	Diffusion coefficient × 10^{10}/ $m^2 \cdot s^{-1}$	R^2
293	0.0656	1.0933	0.9864
303	0.0567	0.9450	0.9893
313	0.0707	1.1783	0.9876
323	0.1067	1.7783	0.9954
333	0.1321	2.2017	0.9939
343	0.1176	1.9600	0.9965
353	0.1701	2.8350	0.9866

Table 2
Summary table of intrinsic diffusion coefficients of DBP

Slope	Intercept	Activation energy/ $kJ \cdot mol^{-1}$	Diffusion coefficient × 10^{8}/ $m^2 \cdot s^{-1}$	R^2
−1817.44	−16.91	15.1102	4.5343	0.866

state is shorter, which simulates the aging process. Fig. 6(d) normalizes the different influencing factors, and we find that almost all the lines can coincide completely. It indicates that our model can well explain the influence of different influencing factors, such as the degree of crystallinity of propellant, the intermolecular interaction, and temperature on the diffusion behavior of DBP in NC. As shown in Fig. 6(d), the system is in equilibrium at about $t/\tau = 0.6$.

3.3. Comparison with experimental detection

To explain that the onion model can effectively predict the concentration distribution of DBP in NC during the aging process, the simulated data are compared with the experimental data, and the concentration distributions of DBP at different temperatures are predicted. Table 3 shows the diffusion coefficients obtained after aging for six days at 328, 338, and 348 K (the specific calculation processes shown in S5). According to the experimental diffusion

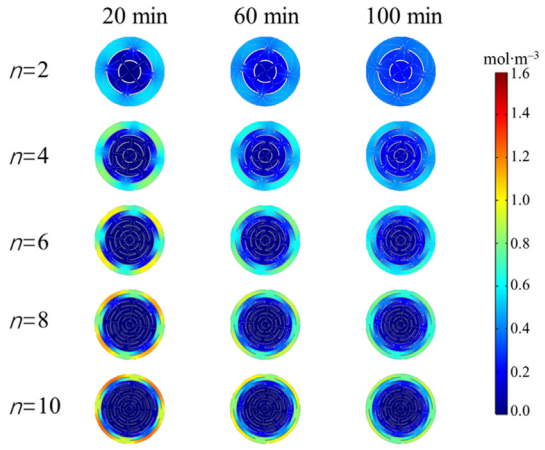

Fig. 3. Concentration distributions of DBP in propellant at different times and layers. The number of holes on each clapboard is 4. The simulated temperature is 298 K.

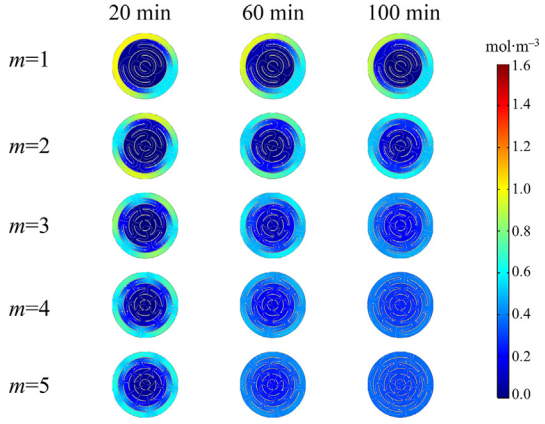

Fig. 4. Concentration distributions of DBP in propellant at different times and different numbers of holes. The simulated temperature is 298 K.

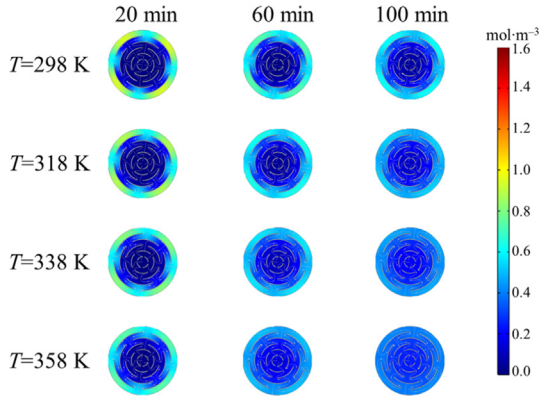

Fig. 5. Concentration distributions of DBP in propellant at different times and different temperatures.

coefficient of 2.2706×10^{-16} at 328 K, 4.997×10^{-16} at 338 K and 8.4745×10^{-16} at 348 K, a series of possible m and n values of the onion model of gun propellant are calculated by Eqs. (3) and (4). Then we select one group of $m = 4$ and $n = 1758$ which is fitted by three groups of experimental data to predict the diffusion behavior of DBP in propellant at 328, 338 and 348 K. The

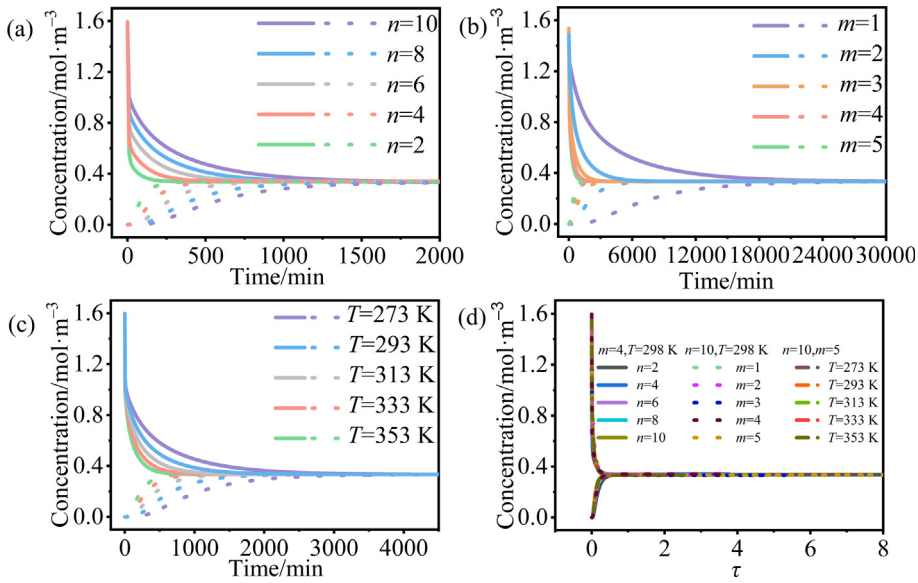

Fig. 6. Variation of maximum and minimum concentrations of DBP with time or characteristic time: (a) when n changes, (b) when m changes, (c) when temperature T changes, (d) when n, m, T changes with characteristic time. In (a)–(c), the solid line represents the change of the highest concentration, and the dotted line represents the change of the lowest concentration.

Table 3
Diffusion coefficients of DBP in NC at different temperatures by experiments

Temperature/K	Diffusion coefficient/m^2·s^{-1}
328	2.2706×10^{-16}
338	4.9970×10^{-16}
348	8.4745×10^{-16}

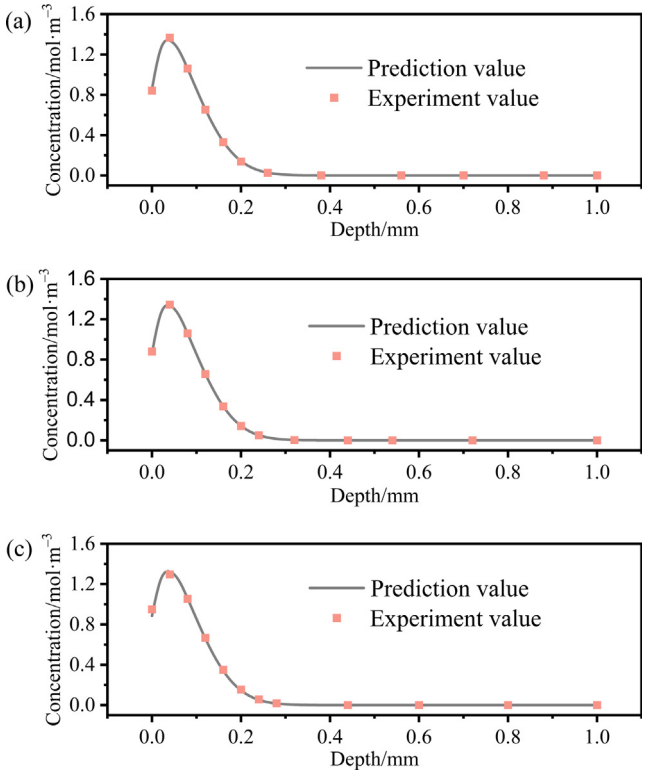

Fig. 7. Comparisons of experiment value and prediction value of DBP concentrations after aging for six days: (a) 338 K, (b) 328 K, (c) 348 K.

results of Fig. 7 show that the concentration distributions of m = 4 and n = 1758 can predict the concentration distribution very well and it is very close to the experimental ones.

The results show that the onion model of propellant can not only normalize the diffusion of DBP under different conditions but also effectively predict the concentration distribution of DBP in NC under different temperature conditions and aging times. Therefore, we can fit the onion model into the propellant through the experimental data, so that we can accurately analyze the concentration distribution of DBP in the propellant after the aging process.

4. Conclusions

Combining molecular dynamics (MD), we put forward the onion model of propellant by analyzing the steric hindrance effect which is caused by crystallization. In this paper, dibutyl phthalate (DBP) was selected as small molecular and nitrocellulose (NC) as main components of propellants. First, we simulated the diffusion of DBP in NC at different temperatures by MD. From 50 ps to 900 ps, MSD has a strong linear relationship with time, satisfying the Einstein–Smoluchowski equation (the correlation coefficient is greater than 0.98). The temperature dependence of the diffusion coefficient follows the Arrhenius equation (the correlation coefficient is 0.866). The diffusion activation energy is 15.1 kJ·mol^{-1}, and the pre-exponential factor is 4.53×10^{-4} m^2·s^{-1}. Then these microscale diffusion data are imported into the onion model, to simulate the diffusion behavior of DBP in the propellant. We simulate the diffusion of different crystalline propellants at different temperatures, and we can get the concentration distribution of DBP in propellants at any time and any position. Then we normalized all the variables by τ, and found that all curves under different conditions end upon the same line. The systems reached equilibrium when t/τ was about 0.6. Finally, we simulated the aging process of six days by Raman spectroscopy and measured the concentration distribution of DBP in NC and the diffusion coefficient at different temperatures. We found that the concentration distribution obtained by the onion model can well fit the experimental concentration distribution.

Although we only focus on the diffusion of DBP in a single-base propellant with NC as the main component, it is believed that the diffusion of the smallest molecule can be applied to the onion model [31]. Because we can build any small molecular in the process of MD simulation, then import the diffusion coefficient data into the onion model. The thicknesses of the outermost clapboard and the innermost clapboard of the onion model are different, which will be compared with the internal crystallization of propellant in the next study to solve this problem. Future research will focus on the diffusion experiments of different small molecules in propellants and the data acquisition of m, n values of propellants with different crystallinity. In the process of using propellant, we can get the real-time deterrent concentration distribution by the onion model. This method of theoretical calculation without experiment will greatly save time and resources, and provide theoretical guidance for the design and modification of propellants.

Data Availability

Data will be made available on request.

Declaration of Competing Interest

The authors declare that they have no known competing financial interests or personal relationships that could have appeared to influence the work reported in this paper.

Acknowledgements

This work was sponsored by the National Natural Science Foundation of China (91834301, 22078088, 22005143) and the National Natural Science Foundation of China for Innovative Research Groups (51621002).

Supplementary Material

Supplementary data to this article can be found online at https://doi.org/10.1016/j.cjche.2022.03.018.

References

[1] H. Singh, H.G. Gokhale, A new stability concept for propellants, *Def. Sci. J.* 35 (4) (1985) 417–423.
[2] P. Ase, W. Eisenberg, S. Gordon, K. Taylor, A. Snelson, Propellant combustion product analyses on an M16 rifle and a 105mm caliber Gun, *J. Environ. Sci. Heal. A Environ. Sci. Eng.* 20 (3) (1985) 337–368.
[3] Q.L. Wang, S.W. Li, Z.S. Wang, Research development for diffusion of deterrent in gun propellant, Chin. J. Explos. Propell. 23 (1) (2000) 14–16. (in Chinese)
[4] S. Pan, Z.Y. Huang, X. Zhang, X.M. Hu, Property improvement on two reactive surface deterrents of azidonitramine gun propellant, Chin. J. Explos. Propell. 41 (1) (2018) 102–106. (in Chinese)
[5] P.Q. Hieu, Regulation of burning speed for the granules of high energy materials in military field (single-based propellant) using absorption of camphor methods, *Vietnam J. Sci. Technol.* 56 (2A) (2018) 51–55.
[6] B.W. Brodman, M.P. Devine, R.W. Finch, M.S. MacClaren, Autoradiographic determination of the di-*n*-butyl phthalate concentration profile in a nitrocellulose matrix, *J. Appl. Polym. Sci.* 18 (12) (1974) 3739–3744.
[7] T. Kairn, P.J. Daivis, I. Ivanov, S.N. Bhattacharya, Molecular-dynamics simulation of model polymer nanocomposite rheology and comparison with experiment, *J. Chem. Phys.* 123 (19) (2005) 194905.
[8] J.S. Wei, Diffusion behavior of small molecule desensitizer in single base propellant, Ph. D. Thesis, Nanjing University of Technology, China, 2012. (in Chinese)
[9] B. Liu, B.M. Zhao, B. Chen, F.S. Ma, Q.L. Wang, S.W. Liu, Research for diffusion of the polymer deterrent in the gun propellant, In: Proceedings of the 31st International Symposium on Ballistics, Hyderabad, India, November 4-8, 2019, pp. 428–434.
[10] J.M. García-Ruiz, F. Otálora, Concentration distribution around a crystal growing under diffusional control: A computer simulation, *J. Cryst. Growth* 118 (1–2) (1992) 160–162.
[11] Y.N. Zheng, Q. Liu, Y. Li, N. Gindy, Investigation on concentration distribution and mass flow rate measurement for gravity chute conveyor by optical tomography system, *Measurement* 39 (7) (2006) 643–654.
[12] H. Takeuchi, K. Okazaki, Molecular dynamics simulation of diffusion of simple gas molecules in a short chain polymer, *J. Chem. Phys.* 92 (9) (1990) 5643–5652.
[13] P.A. Zhang, T.Q. Li, S.M. Liu, J.R. Deng, Effects of NPBA on interface interaction and mechanical properties of NEPE propellant: Insight from molecular dynamics simulation, *Comp. Mater. Sci.* 171 (2020) 109135.
[14] Y.F. Ding, H. Liang, Y.J. Ding, Z.L. Xiao, Molecular dynamics simulation of DBP and NA diffusion properties in gun propellant, Chin. J. Energ. Mater. 29 (1) (2021) 65–73. (in Chinese)
[15] P.G. de Gennes, Introduction to Polymer Dynamics, Cambridge University Press, Cambridge, 1990.
[16] B.W. Brodman, J.A. Sipia, S. Schwartz, Diffusion of deterrents into a nitrocellulose matrix. An example of diffusion with interaction, *J. Appl. Polym. Sci.* 19 (7) (1975) 1905–1909.
[17] R. Eshaghi Malekshah, B. Fahimirad, M. Aallaei, A. Khaleghian, Synthesis and toxicity assessment of Fe_3O_4 NPs grafted by approximately NH_2-Schiff base as anticancer drug: Modeling and proposed molecular mechanism through docking and molecular dynamic simulation, *Drug Deliv.* 27 (1) (2020) 1201–1217.
[18] E. Rocco, The COMPASS future: COMPASS II, *Prog. Part. Nucl. Phys.* 67 (2) (2012) 288–293.
[19] S.R. Anderson, D.J. Am Ende, J.S. Salan, P. Samuels, Preparation of an energetic-energetic cocrystal using resonant acoustic mixing, *Propell. Explos. Pyrot.* 39 (5) (2014) 637–640.
[20] A.N. Pour, M. Zare, Y. Zamani, Studies on product distribution of alkali promoted iron catalyst in Fischer-Tropsch synthesis, *J. Nat. Gas Chem.* 19 (2010) 31–34.
[21] Y.J. Ding, S. Zhang, S.J. Ying, Z.L. Xiao, Fabrication and combustion properties of TEGN/RDX based microcellular combustible objects, Chin. J. Explos. Propell. 42 (4) (2019) 25–30. (in Chinese)
[22] L.G. Wang, L.I. Xiao-Jiang, B. Kang, J. Zhao, Z.W. Song, Research on crystallization behavior of NC/PEG blends, Initiators Pyrotech. (5) (2012) 44–47. (in Chinese)
[23] D.N. Saheb, J.P. Jog, Crystallization and equilibrium melting behavior of PBT/PETG blends, *J. Polym. Sci. B Polym. Phys.* 37 (17) (1999) 2439–2444.
[24] M.H. Kong, D.X. Wu, X.B. Chen, Qualitative and quantitative studies on artemisinin with Raman spectroscopy, Spectrosc. Spect. Anal. 37 (3) (2017) 778–782. (in Chinese)
[25] N.N. Zhang, Z.R. Zheng, C.C. Han, Solvent concentration distribution in acetone/PMMA coating solution measured by laser confocal Raman spectroscopy method, *Laser Optoelectron. Prog.* 54 (12) (2017) 123101.
[26] M. Schwaab, J.C. Pinto, Optimum reference temperature for reparameterization of the Arrhenius equation. Part 1: Problems involving one kinetic constant, *Chem. Eng. Sci.* 62 (10) (2007) 2750–2764.
[27] S. Hofmann, G. Csányi, A.C. Ferrari, M.C. Payne, J. Robertson, Surface diffusion: The low activation energy path for nanotube growth, *Phys. Rev. Lett.* 95 (3) (2005) 036101.
[28] Q. Jiang, S.H. Zhang, J.C. Li, Grain size-dependent diffusion activation energy in nanomaterials, *Solid State Commun.* 130 (9) (2004) 581–584.
[29] M. Okubo, Y. Tanaka, H.S. Zhou, T. Kudo, I. Honma, Determination of activation energy for Li ion diffusion in electrodes, *J. Phys. Chem. B* 113 (9) (2009) 2840–2847.
[30] B. Vogelsanger, B. Ossola, E. Brönnimann, The diffusion of deterrents into propellants observed by FTIR microspectroscopy—Quantification of the diffusion process, *Propell. Explos. Pyrot.* 21 (6) (1996) 330–336.
[31] P. Demontis, J. Kärger, G.B. Suffritti, A. Tilocca, Application of the two-step model to the diffusion of linear diatomic and triatomic molecules in silicalite, *Phys. Chem. Chem. Phys.* 2 (7) (2000) 1455–1463.